

Compressive Beam-Pattern–Aware Near-field Beam Training via Total Variation Denoising

Zijun Wang, Maria Nivetha A, Ye Hu, *Member, IEEE*, Rui Zhang, *Member, IEEE*

Abstract—Extremely large antenna arrays envisioned for 6G incurs near-field effect, where steering vector depends on angles and range simultaneously. Polar-domain near-field codebooks can focus energy accurately but incur extra two-dimensional sweeping overhead; compressed-sensing (CS) approaches with Gaussian-masked DFT sensing offer a lower-overhead alternative. This letter revisits near-field beam training using conventional DFT codebooks. Unlike far-field responses that concentrate energy on a few isolated DFT beams, near-field responses produce contiguous, plateau-like energy segments with sharp transitions in the DFT beamspace. Pure LASSO denoising, therefore, tends to over-shrink magnitudes and fragment plateaus. We propose a beam-pattern–preserving beam training scheme for multiple-path scenarios that combines LASSO with a lightweight denoising pipeline: LASSO to suppress small-amplitude noise, followed by total variation (TV) to maintain plateau levels and edge sharpness. The two proximal steps require no near-field codebook design. Simulations with Gaussian pilots show consistent NMSE and cosine-similarity gains over least squares and LASSO at the same pilot budget.

Index Terms—near-field, beam training, compressive sensing, total variation denoising, mmWave/THz, beam pattern

I. INTRODUCTION

THE imminent 6G era will exploit a broadened spectrum portfolio that extends beyond traditional sub-6 GHz bands to the emerging upper mid-band/FR3 (7–24 GHz), while also leveraging mmWave and sub-THz bands to support multi-Gbps connectivity and new services [1], [2], [3]. To compensate for increased propagation loss at higher frequencies, extremely large antenna arrays (ELAA) with hundreds to thousands of elements are expected, which incur the radiative near-field effect in wireless networks [4]. Unlike the far-field (i.e., plane-wave) model, where steering vectors depends only on angle, the near-field channel model exhibits spherical wavefronts and steering vectors that depend on both angle and range [5], [6].

This shift motivated extensive research on channel modeling, beam training, and channel estimation in the near-field region [7], [8]. Some works directly extend conventional far-field beam-training schemes to near-field line-of-sight (LoS) links [9], [10]. [9] estimates the angle via a DFT codebook

Zijun Wang, Maria Nivetha A and Rui Zhang are with the Department of Electrical Engineering, The State University of New York at Buffalo, New York, USA (email: zwang267@buffalo.edu, marianniv@buffalo.edu, rzhang45@buffalo.edu).

Ye Hu is with the Industrial and Systems Engineering, and Department of Electrical and Computer Engineering, University of Miami, Florida, USA (email: yehu@miami.edu).

This work was supported in part by the CSD, MediaTek Inc. USA, under Grant 103764, and in part by the National Science Foundation, under Grant ECCS 2512911.

and then performs a range search conditioned on the estimated direction, whereas [10] uses DFT sweeping and jointly estimates angle and range from received power measurements. Moreover, [7] develops a polar-domain codebook that embeds both angular and range information for uplink channel estimation. While such polar-domain codebooks enable accurate near-field beam focusing, their two-dimensional sampling over the distance and angle domain inevitably enlarges the beam-sweeping set and thus inflates the training and the storage overhead. Also, such codebook is not supported by the angle-only CSI codebook framework in current standard [11]. Motivated by conventional far-field channel estimation, it is natural instead to regard the near-field channel as sparse in a suitable transform domain and adopt compressive sensing (CS) to estimate the corresponding coefficients. Classical CS theory shows that random-masked Fourier operators provide stable recovery via LASSO under Restricted Isometry Property (RIP) and related incoherence conditions [12], [13]. For example, [14] formulates channel estimation as a sparse recovery problem and applies orthogonal matching pursuit (OMP) to identify the dominant AoA/AoD components under hybrid beamforming constraints. More generally, [15] proposes a compressive channel estimation framework applicable across different hybrid hardware realizations. In contrast, sensing built from highly focused near-field codewords is typically much more coherent and thus lacks RIP-type guarantees [16].

Because of the mismatch between polar-domain near-field codebooks and classical compressed sensing, we explore using conventional DFT codebooks that are typically used in far-field users as a low-overhead CS approach to near-field beam training. Near-field effects cause energy to split across neighboring DFT beams [7], [17], but when scattering is limited (e.g., higher frequency band), the channel can still be accurately captured by a small number of DFT codewords, preserving sparsity that CS methods exploit [18]. Consequently, near-field DFT-beamspace responses form contiguous, plateau-like regions rather than isolated peaks[19]. Standard LASSO regularization commonly over-shrinks coefficient magnitudes and encourages isolated nonzeros, which can break up or attenuate such plateaus. Total variation (TV) denoising, however, encourages piecewise-constant solutions and preserves sharp transitions, so combining LASSO with TV naturally suits beamspace patterns that are both sparse and plateau-structured [20].

Motivated by these insights, this letter proposes a low-overhead compressive training framework that pairs Gaussian-masked DFT sensing with a two-stage denoising pipeline: LASSO to suppress small-amplitude noise, followed by TV

denoising to preserve plateau heights and sharp transitions. The proposed approach requires no specialized near-field codebook and is applicable to both ULA (uniform linear array) and UPA (uniform planar array) configurations. Importantly, our method can be implemented directly on top of existing DFT-based codebook architectures, enabling compatibility with current standard-compliant transceivers [11].

The rest of the paper is organized as follows. Section II introduces the near-field system model for a UPA. Section III analyzes the DFT beam patterns and the resulting sparsity structure. Section IV presents the proposed compressive beam training algorithm. Section V reports simulation results for the UPA scenario. Finally, Section VI concludes the paper.

II. SYSTEM MODEL

We consider a downlink narrowband system where a base station (BS) is equipped with an $N_y \times N_z$ uniform planar array (UPA) serving a single-antenna user. The UPA lies on the y - z plane and is centered at the origin. Each user terminal is equipped with a single antenna. The carrier frequency is denoted by f_c and the corresponding wavelength is $\lambda = c/f_c$, with c being the speed of light. We focus on the radiative near-field regime where the user range lies between the Fresnel distance r_F and the Rayleigh distance r_R [8]. The whole system is shown in Fig. 1.

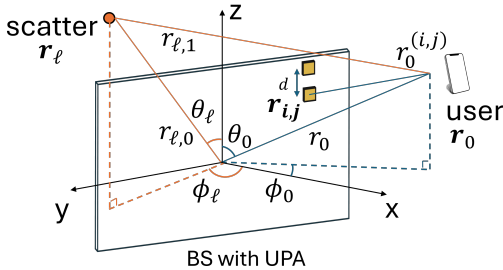


Fig. 1. Diagram of the near-field communication system featuring a UPA.

Let $\mathcal{N}_y \triangleq \{0, 1, \dots, N_y - 1\}$, $\mathcal{N}_z \triangleq \{0, 1, \dots, N_z - 1\}$, and define centered index offsets $\delta_i \triangleq \frac{2i - N_y + 1}{2}$, $\delta_j \triangleq \frac{2j - N_z + 1}{2}$, $i \in \mathcal{N}_y$, $j \in \mathcal{N}_z$. The (i, j) -th antenna element is located at $\mathbf{r}_{i,j} = (0, \delta_i d, \delta_j d)^\top$, where the inter-element spacing is $d = \lambda/2$ and the total number of antennas is $N \triangleq N_y N_z$.

A point in space (i.e., user or scatterer) is described in spherical coordinates by range $r > 0$, elevation angle $\theta \in [0, \pi]$ and azimuth angle $\phi \in [-\pi, \pi]$. We adopt the unit direction vector

$$\mathbf{q}(\theta, \phi) \triangleq \begin{bmatrix} \sin \theta \cos \phi \\ \sin \theta \sin \phi \\ \cos \theta \end{bmatrix}, \quad (1)$$

so that the Cartesian position of a point at (θ, ϕ, r) is $r \mathbf{q}(\theta, \phi)$. The distance between this point and the (i, j) -th array element is $r^{(i,j)}(\theta, \phi, r) = \|r \mathbf{q}(\theta, \phi) - \mathbf{r}_{i,j}\|_2$. The corresponding near-field steering response of this path on the UPA is

$$[b(\theta, \phi, r)]_{i,j} = \frac{1}{\sqrt{N}} \exp\left(-j \frac{2\pi}{\lambda} (r^{(i,j)}(\theta, \phi, r) - r)\right), \quad (2)$$

and stacking all (i, j) into a fixed order yields the steering vector $\mathbf{b}(\theta, \phi, r) \in \mathbb{C}^N$.

We assume a single-antenna user is located at (θ_0, ϕ_0, r_0) , where r_0 is the distance between user and BS. The LoS component is modeled as

$$\mathbf{h}_0 = \sqrt{N} g_0 e^{-j \frac{2\pi r_0}{\lambda}} \mathbf{b}(\theta_0, \phi_0, r_0), \quad (3)$$

with large-scale gain $g_0 = \frac{\lambda}{4\pi r_0}$.

In addition, we consider $(L - 1)$ single-bounce scatterers indexed by $\ell = 1, \dots, L - 1$. The ℓ -th scatterer is located at $(\theta_\ell, \phi_\ell, r_{\ell,0})$ with respect to the BS, so its position vector is $\mathbf{r}_\ell \triangleq r_{\ell,0} \mathbf{q}(\theta_\ell, \phi_\ell)$. The BS-scatter distance is therefore $r_{\ell,0} = \|\mathbf{r}_\ell\|_2$, and the scatter-user distance is $r_{\ell,1} = \|r_0 \mathbf{q}(\theta_0, \phi_0) - r_{\ell,0} \mathbf{q}(\theta_\ell, \phi_\ell)\|_2$. The NLoS contribution of the ℓ -th path is modeled as

$$\mathbf{h}_\ell = \sqrt{N} g_\ell e^{-j \frac{2\pi (r_{\ell,0} + r_{\ell,1})}{\lambda}} \mathbf{b}(\theta_\ell, \phi_\ell, r_{\ell,0}), \quad (4)$$

where $g_\ell = \frac{\lambda}{4\pi r_{\ell,0} r_{\ell,1}} p_\ell$, $p_\ell \sim \mathcal{CN}(0, 1)$, captures both the two-hop path loss and the random complex reflection coefficient of the ℓ -th scatterer. Collecting the LoS and NLoS contributions, the overall downlink channel is

$$\mathbf{h} = \mathbf{h}_0 + \sum_{\ell=1}^{L-1} \mathbf{h}_\ell \in \mathbb{C}^N. \quad (5)$$

III. ANALYSIS OF BEAM PATTERN

This section characterizes how a near-field path appears in the 2D DFT beamspace of a UPA. In contrast to the far-field case where energy concentrated on a single DFT index, near-field Fresnel phases spread the energy over a connected neighborhood, forming plateau-like regions with sharp edges. We first show that, under a separable Fresnel approximation, the 2D beam pattern of UPA factorizes into two 1D uniform linear array (ULA) patterns, and then use the 6-dB lobe width law of ULA in [17] to quantify the per-axis spreading widths and the resulting effective sparsity.

We define the two DFT spatial variables $u \triangleq \sin \theta \sin \phi$, $v \triangleq \cos \theta$. With this parameterization, the 2D DFT sampling that ensures orthogonality corresponds to uniform grids on (u, v) , i.e., $u_n = \frac{2n - N_y + 1}{N_y}$, $v_m = \frac{2m - N_z + 1}{N_z}$, for DFT indices $n \in \{0, \dots, N_y - 1\}$ and $m \in \{0, \dots, N_z - 1\}$.

We adopt the standard DFT codebook as the beamspace basis on the UPA. Along the y -axis, for any spatial consine $u \in [-1, 1]$ we define the unit-norm 1D DFT vector

$$\mathbf{a}_y(u) \triangleq \frac{1}{\sqrt{N_y}} [e^{-j \frac{2\pi}{\lambda} du \delta_0}, e^{-j \frac{2\pi}{\lambda} du \delta_1}, \dots, e^{-j \frac{2\pi}{\lambda} du \delta_{N_y-1}}]^\top, \quad (6)$$

and similarly along the z -axis

$$\mathbf{a}_z(v) \triangleq \frac{1}{\sqrt{N_z}} [e^{-j \frac{2\pi}{\lambda} dv \delta_0}, e^{-j \frac{2\pi}{\lambda} dv \delta_1}, \dots, e^{-j \frac{2\pi}{\lambda} dv \delta_{N_z-1}}]^\top, \quad (7)$$

Thus, a 2D DFT codeword on the UPA pointing to (u_n, v_m) is defined by the Kronecker product $\mathbf{a}(u_n, v_m) \triangleq \mathbf{a}_y(u_n) \otimes \mathbf{a}_z(v_m) \in \mathbb{C}^{N_y N_z}$.

A. Separable Fresnel approximation

Let $r^{(i,j)}$ denote the distance from element (i, j) to a path at (θ, ϕ, r) . A second-order (Fresnel) expansion around the array center yields

$$\begin{aligned} r^{(i,j)} - r \approx & -d(u \delta_i + v \delta_j) + \frac{d^2}{2r} \left((1 - u^2) \delta_i^2 + (1 - v^2) \delta_j^2 \right) \\ & - \frac{d^2}{r} u v \delta_i \delta_j. \end{aligned} \quad (8)$$

Following standard large-array UPA codebook analyses [8], the mixed quadratic term $-\frac{d^2}{r}uv\delta_i\delta_j$ is much smaller than the dominant axis-wise terms over the operational near-field region and can be safely neglected. The resulting near-field phase thus approximately separates along the y - and z -axes, and the steering vector becomes separable:

$$\mathbf{b}(u, v, r) \approx \mathbf{b}_y(u, r) \otimes \mathbf{b}_z(v, r), \quad (9)$$

where

$$[\mathbf{b}_y(u, r)]_i = \frac{1}{\sqrt{N_y}} \exp\left\{-j\frac{2\pi}{\lambda}\left(-du\delta_i + \frac{d^2}{2r}(1-u^2)\delta_i^2\right)\right\}, \quad (10)$$

$$[\mathbf{b}_z(v, r)]_j = \frac{1}{\sqrt{N_z}} \exp\left\{-j\frac{2\pi}{\lambda}\left(-dv\delta_j + \frac{d^2}{2r}(1-v^2)\delta_j^2\right)\right\}. \quad (11)$$

B. 2D beam-pattern factorization and plateau support

Let one of the true paths be (u_0, v_0, r_0) . Under the separable Fresnel model Eq. (9), the beam pattern between the near-field steering vector and a 2D DFT codeword factorizes as

$$\begin{aligned} G(u_0, v_0, r_0; u_n, v_m) &\triangleq |\mathbf{b}(u_0, v_0, r_0)^H \mathbf{a}(u_n, v_m)| \\ &\approx |\mathbf{b}_y(u_0, r_0)^H \mathbf{a}_y(u_n)| |\mathbf{b}_z(v_0, r_0)^H \mathbf{a}_z(v_m)|. \end{aligned} \quad (12)$$

Hence, the 2D magnitude response is the product of two 1D responses.

We now separately analyse the beam pattern for 2 directions. To quantify the 1D spreading, define the axis-wise normalized responses for z -axis

$$G_{z,\text{norm}}(v_0, r_0; v) \triangleq \frac{|\mathbf{b}_z(v_0, r_0)^H \mathbf{a}_z(v)|}{|\mathbf{b}_z(v_0, r_0)^H \mathbf{a}_z(v_0)|}. \quad (13)$$

The corresponding 6-dB lobe sets are

$$\Phi_{6\text{dB}}^z(v_0, r_0) \triangleq \{v \mid G_{z,\text{norm}}(v_0, r_0; v) \geq 1/2\}, \quad (14)$$

and the associated widths are

$$B_z(v_0, r_0) \triangleq \max(\Phi_{6\text{dB}}^z) - \min(\Phi_{6\text{dB}}^z). \quad (15)$$

For y -axis the definition is the same.

In the near-field ULA analysis [17], the 6-dB lobe width for a path at (ξ_0, r_0) has the closed-form as

$$B(\xi_0, r_0) = Nd \frac{1 - \xi_0^2}{r_0}. \quad (16)$$

In our UPA setting, for a given path located at (u_0, v_0, r_0) , the separable Fresnel model in Eq. (11) shows that $\mathbf{b}_y(u_0, r_0)$ and $\mathbf{b}_z(v_0, r_0)$ have the same quadratic-phase structure as the near-field ULA steering vector in [17], with apertures $N_y d$ and $N_z d$. The same 6-dB width law applies along each axis, yielding the per-axis spreading widths around the true spatial variables u_0 and v_0 :

$$B_y(u_0, r_0) = N_y d \frac{1 - u_0^2}{r_0}, \quad B_z(v_0, r_0) = N_z d \frac{1 - v_0^2}{r_0}. \quad (17)$$

These widths quantify how far in the continuous (u, v) domain the near-field energy of this path spreads from its peak along each axis due to the near-field quadratic phase. Combined with the factorization in Eq. (12), a convenient and support approximation is given by the Cartesian product of the two

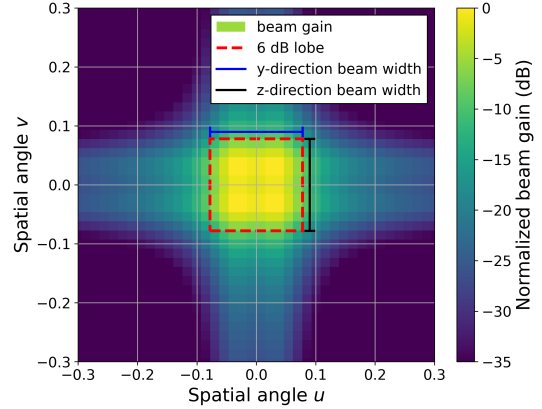


Fig. 2. Normalized DFT-beamspace magnitude on a (128×128) UPA at $f_c = 28$ GHz.

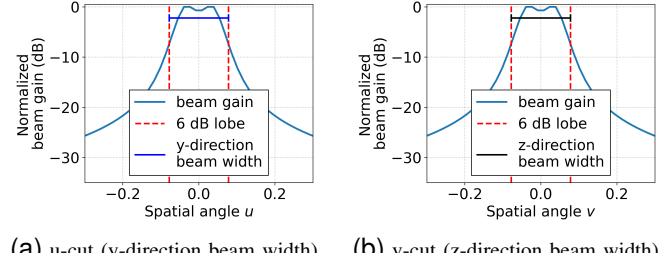


Fig. 3. 1D cuts of the normalized gain and the 6-dB lobe widths.

axis-wise 6-dB sets, which matches the connected plateau with sharp edges observed in DFT beamspace [7], [17].

An example of the UPA beam pattern is shown in Fig. 2. The red dashed rectangle marks the 6-dB lobe region, defined as the set of DFT beam indices whose magnitude exceeds 0.5 of the central peak, and highlights the compact plateau induced by near-field effect. Fig. 3 further shows the 1D u - and v -cuts through the peak of Fig. 2; the 6-dB thresholds (red dashed lines) delineate the per-axis lobe widths B_y and B_z , confirming the flat-top plateau behavior.

C. Effective sparsity level in 2D DFT beamspace

Let Δ_y and Δ_z denote the DFT grid spacings along the u - and v -axes, respectively. Approximating each path's 2D lobe support by a rectangle with side lengths B_y and B_z , the number of active DFT coefficients per path is approximately $B_y B_z / (\Delta_y \Delta_z)$. For L paths with non-overlapping lobe supports (the worst case), the expected sparsity level K_{UPA} (i.e., the expected number of active DFT coefficients) scales as

$$\mathbb{E}[K_{\text{UPA}}] \approx \frac{LN_y N_z d^2}{\Delta_y \Delta_z} \mathbb{E}\left[\frac{(1-u^2)(1-v^2)}{r^2}\right]. \quad (18)$$

Note that u and v are coupled through $u = \sin \theta \sin \phi = \sqrt{1-v^2} s$ with $s \triangleq \sin \phi$. For typical near-field user distributions, the expectation in Eq. (18) can be evaluated in closed form. For a $N_y \times N_z = 128 \times 16$ UPA at $f_c = 28$ GHz with $d = \lambda/2$ and the standard 2D DFT grid $\Delta_y = 2/N_y$ and $\Delta_z = 2/N_z$, consider $v \sim \mathcal{U}[-\frac{1}{2}, \frac{1}{2}]$, $s \sim \mathcal{U}[-\frac{1}{2}, \frac{1}{2}]$, $r \sim \mathcal{U}[r_F, \frac{r_R}{20}]$. In this case, for an $L = 5$ -path channel, Eq. (18) yields $\mathbb{E}[K_{\text{UPA}}] \approx 8.6$, confirming that the near-field channel remains strongly sparse in the 2D DFT beamspace under this setting.

This analysis suggests that the near-field 2D DFT coefficients are not only sparse but also clustered into compact, plateau-like lobe supports with sharp boundaries. A pure LASSO tends to induce amplitude bias and favors scattered nonzeros, which can erode flat lobe levels and break a contiguous block into fragmented patches. In contrast, TV regularization promotes piecewise-constant structure within each lobe while preserving edge discontinuities, making it a natural complement to LASSO for denoising near-field DFT beamspace patterns.

IV. COMPRESSIVE BEAM TRAINING

We present a multi-stage compressive beam training method motivated by the near-field DFT beam patterns in Section III. Consider an $N_y \times N_z$ UPA and denote the column-stacked array-domain channel by $\mathbf{h} \in \mathbb{C}^N$ with $N \triangleq N_y N_z$. Define the unitary 2D DFT basis without oversampling as $\mathbf{F} \in \mathbb{C}^{N \times N}$. We represent the channel in the 2D DFT beamspace as $\mathbf{h} = \mathbf{F}\mathbf{s}$, where $\mathbf{s} \in \mathbb{C}^N$ is the beamspace coefficient vector. To expose the 2D structure, we reshape \mathbf{s} into a matrix $\mathbf{S} \in \mathbb{C}^{N_y \times N_z}$ using the same column-stacking order, i.e., $\mathbf{s} = \text{vec}(\mathbf{S})$.

During training, the BS transmits M pilot beams $\{\mathbf{v}_m\}_{m=1}^M$ with $M \ll N$, each generated as a masked 2D-DFT combination $\mathbf{v}_m = \mathbf{F}\mathbf{p}_m$, $\mathbf{p}_m \sim \mathcal{CN}(\mathbf{0}, \frac{1}{N}\mathbf{I}_N)$. With pilot $x = 1$, the received observation is $y_m = \mathbf{h}^H \mathbf{v}_m + w_m = \mathbf{s}^H \mathbf{p}_m + w_m$, where $w_m \sim \mathcal{CN}(0, \sigma^2)$. Stacking $\{y_m\}$ yields the linear beamspace model

$$\mathbf{y} = \Phi \mathbf{s} + \mathbf{w}, \quad \Phi \triangleq \begin{bmatrix} \mathbf{p}_1^H \\ \vdots \\ \mathbf{p}_M^H \end{bmatrix} \in \mathbb{C}^{M \times N}. \quad (19)$$

As shown in Section III, a near-field path produces a compact, plateau-like lobe in the 2D DFT beamspace. This motivates a three-stage beam training scheme.

1) Stage I: support detection via LASSO

We first obtain a coarse estimate by solving

$$\hat{\mathbf{s}}^{(\ell_1)} \in \arg \min_{\mathbf{s} \in \mathbb{C}^N} \frac{1}{2} \|\mathbf{y} - \Phi \mathbf{s}\|_2^2 + \lambda_1 \|\mathbf{s}\|_1. \quad (20)$$

Reshape $\hat{\mathbf{s}}^{(\ell_1)}$ into $\hat{\mathbf{S}}^{(\ell_1)} \in \mathbb{C}^{N_y \times N_z}$ via the $\text{vec}(\cdot)$ order, and form an initial support mask by top- k selection on magnitudes:

$$\mathcal{M}_0 = \text{Top-}k(|\hat{\mathbf{S}}^{(\ell_1)}|) \subseteq \{1, \dots, N_y\} \times \{1, \dots, N_z\}. \quad (21)$$

2) Stage II: 2D support dilation

To capture the full connected lobe support, we dilate \mathcal{M}_0 by a 2D radius $(r_y, r_z) \in \mathbb{N}^2$:

$$\widetilde{\mathcal{M}} = \left\{ (i, j) \mid \exists (i', j') \in \mathcal{M}_0 \text{ s.t. } |i - i'| \leq r_y, |j - j'| \leq r_z \right\}. \quad (22)$$

3) Stage III: magnitude-TV refinement on the dilated mask

We refine the beamspace coefficients on $\widetilde{\mathcal{M}}$ by penalizing the 2D total variation of the magnitude map $|\mathbf{S}|$:

$$\begin{aligned} \widehat{\mathbf{S}} \in \arg \min_{\mathbf{S} \in \mathbb{C}^{N_y \times N_z}} & \frac{1}{2} \|\mathbf{y} - \Phi \text{vec}(\mathbf{S})\|_2^2 + \lambda_{\text{TV}} \text{TV}_{2D}(|\mathbf{S}|; \widetilde{\mathcal{M}}) \\ \text{s.t.} & \quad S_{i,j} = 0, \quad \forall (i,j) \notin \widetilde{\mathcal{M}}. \end{aligned} \quad (23)$$

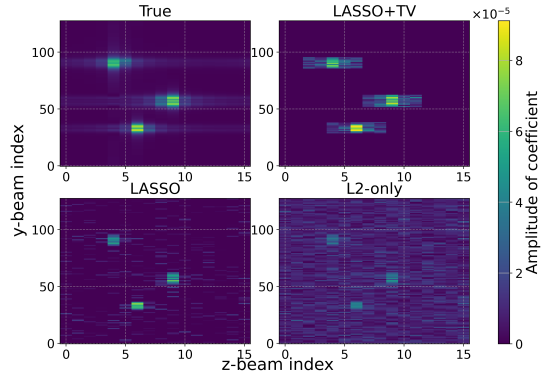


Fig. 4. DFT beamspace magnitude on a UPA near-field channel.

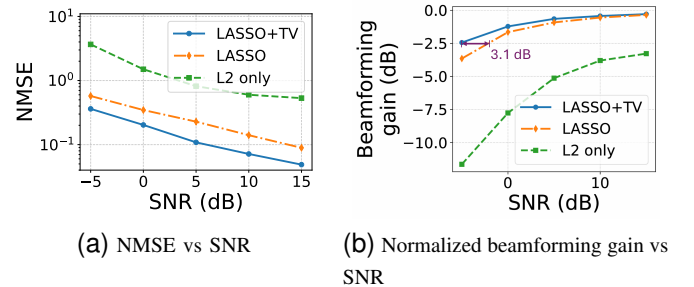


Fig. 5. Simulation results for the SNR sweeping.

We use the anisotropic masked TV

$$\text{TV}_{2D}(|\mathbf{S}|; \widetilde{\mathcal{M}}) = \sum_{(i,j) \in \widetilde{\mathcal{M}}} |S_{i+1,j}| - |S_{i,j}| + \sum_{(i,j) \in \widetilde{\mathcal{M}}} |S_{i,j+1}| - |S_{i,j}|, \quad (24)$$

where out-of-range terms are ignored at the boundaries. The final beamspace estimate is $\hat{\mathbf{s}} = \text{vec}(\hat{\mathbf{S}})$. We recover the array-domain channel via $\hat{\mathbf{h}} = \mathbf{F}\hat{\mathbf{s}}$. Finally, we form the beamforming vector by normalizing the recovered channel $\hat{\mathbf{v}} = \hat{\mathbf{h}}/\|\hat{\mathbf{h}}\|_2$.

V. SIMULATION RESULTS

We consider a single BS equipped with a UPA of $N_y = 128$, $N_z = 16$ antenna elements and the central frequency is $f_c = 28\text{GHz}$. We first plot comparison of recovered channel coefficients power of different methods. We consider a multipath channel with $L = 3$ and SNR=0 dB. As shown in Fig. 4, the true beamspace exhibits a compact 2D plateau centered around each path, consistent with the separable near-field lobe structure discussed in Section III. The proposed LASSO+TV estimator closely matches both the extent and the height of this plateau while strongly suppressing out-of-support leakage. In contrast, pure LASSO produces a fragmented, ridge-like pattern with over-shrunk amplitudes and spurious side patches, whereas the L2-only baseline is dominated by diffuse noise spread over the entire beamspace. This proves that LASSO+TV restores a clean rectangular lobe block that aligns with the expected UPA near-field beam pattern, while LASSO and L2 fail to recover a clear 2D support.

We next consider Monte Carlo simulations with $N_{\text{user}} = 500$ independent user channels, each modeled as an $L = 5$ -path near-field link with uniform random location (u, s, r) in the UPA near-field region. The NMSE and averaging normalized beamforming gain are shown in Figs. 5a and 5b.

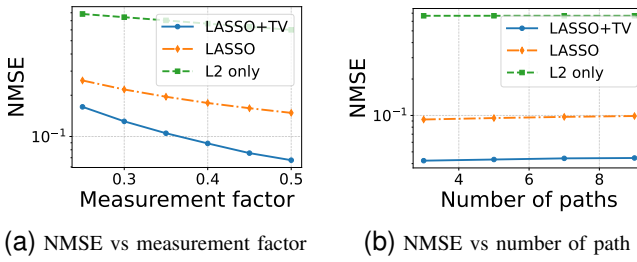


Fig. 6. Simulation results for the pilot-budget and path-number sweeping.

For each realization, we sweep the downlink SNR from -5 dB to 15 dB. The per-realization NMSE and normalized beamforming gain(dB) are defined as $\text{NMSE}(\hat{\mathbf{h}}, \mathbf{h}) \triangleq \frac{\|\hat{\mathbf{h}} - \mathbf{h}\|_2^2}{\|\mathbf{h}\|_2^2}$, $\rho(\hat{\mathbf{h}}, \mathbf{h}) \triangleq 20 \log_{10} \left(\frac{\|\hat{\mathbf{h}}^H \mathbf{h}\|}{\|\hat{\mathbf{h}}\|_2 \|\mathbf{h}\|_2} \right)$.

From Fig. 5a, the proposed LASSO+TV estimator consistently achieves the lowest NMSE across the whole SNR range. At low SNR, it reduces NMSE by about 16% over LASSO and about 87% over the L2-only baseline. At medium SNR, the corresponding NMSE reductions are about 32% and 84%, respectively, and at high SNR the gains remain substantial (about 27% over LASSO and 88% over L2-only).

The mean normalized beamforming gain in Fig. 5b further demonstrates a consistent advantage of LASSO+TV. In particular, at $\text{SNR} = 0$ dB, LASSO+TV achieves a gain of -1.22 dB, which is about 0.43 dB higher than plain LASSO and about 6.55 dB higher than L2-only. At $\text{SNR} = 15$ dB, LASSO+TV improves to -0.29 dB, remaining about 0.06 dB above LASSO and about 2.99 dB above L2-only. Overall, at the -2.5 dB beamforming-gain level, LASSO+TV provides an effective SNR gain of about 3.1 dB over plain LASSO, confirming that enforcing both sparsity and plateau-preserving local smoothness in the DFT beamspace translates into robust beamforming gains in the UPA setting.

We next study the impact of pilot budget under the same UPA setting and set $\text{SNR} = 10$ dB. The measurement factor M/N is swept from 0.25 to 0.50 , corresponding to $M = 512$ – 1024 pilots. From Fig. 6a, increasing M/N improves all methods, and LASSO+TV is uniformly best. At $M/N = 0.25$, LASSO+TV attains $\text{NMSE} = 2.19 \times 10^{-1}$, which is lower than LASSO by 3.69×10^{-2} , corresponding to a 14% NMSE reduction, and lower than L2-only by 5.64×10^{-1} , corresponding to a 72% NMSE reduction. At $M/N = 0.50$, LASSO+TV reduces NMSE by 40% relative to LASSO, and by 85% relative to L2-only.

In Fig. 6b, we evaluate the impact of the number of paths L on channel recovery performance. As L increases, all methods exhibit a slight degradation, consistent with the reduced sparsity of the DFT-beamspace representation under richer multipath. Nevertheless, the proposed LASSO+TV remains consistently superior to plain LASSO across the entire range of L , providing a stable NMSE reduction of roughly 35%–40%. This highlights the necessity of exploiting beamspace sparsity and plateau structure for reliable near-field recovery.

VI. CONCLUSION

In this paper, we studied near-field beam training for multiple-path scenarios using conventional DFT codebooks and low-overhead Gaussian-masked DFT pilots. Motivated by

the plateau-like near-field DFT beam patterns, we proposed a LASSO–dilation–magnitude-TV refinement that exploits clustered sparsity and preserves lobe edges without designing polar-domain codebooks. Simulations for UPA near-field multipath channels show consistent NMSE and beamforming-correlation gains over least squares and plain LASSO. In the considered UPA setting, the proposed method achieves about a 2–3 dB effective SNR gain over LASSO.

REFERENCES

- [1] H. Miao et al., “6G new Mid-Band/FR3 (6–24 GHz): Channel measurement, characteristics and modeling,” *IEEE Open Journal of the Communications Society*, vol. 6, pp. 9942–9960, 2025.
- [2] S. Kang, G. Geraci, M. Mezzavilla, and S. Rangan, “Cellular wireless networks in the upper mid-band,” *IEEE Open Journal of the Communications Society*, vol. 5, pp. 2058–2075, 2024.
- [3] M. Zhang et al., “New mid-band for 6G: Several considerations from the channel propagation characteristics perspective,” *IEEE Communications Magazine*, vol. 63, no. 1, pp. 175–180, Jan. 2025.
- [4] H. Lu et al., “A tutorial on near-field xl-mimo communications towards 6G,” *IEEE Communications Surveys & Tutorials*, vol. 26, no. 4, pp. 2213–2257, 2024.
- [5] X. Wei and L. Dai, “Channel estimation for extremely large-scale massive mimo: Far-field, near-field, or hybrid-field?” *IEEE Commun. Lett.*, vol. 26, no. 1, pp. 177–181, Jan. 2022.
- [6] Y. Liu, Z. Wang, J. Xu, C. Ouyang, X. Mu, and R. Schober, “Near-field communications: A tutorial review,” *IEEE Open J. Commun. Soc.*, vol. 4, pp. 1999–2049, Aug. 2023.
- [7] M. Cui and L. Dai, “Channel estimation for extremely large-scale mimo: Far-field or near-field?” *IEEE Trans. Commun.*, vol. 70, no. 4, pp. 2663–2677, Apr. 2022.
- [8] Z. Wu and L. Dai, “Multiple Access for Near-Field Communications: SDMA or LDMA?” *IEEE Journal on Selected Areas in Communications*, vol. 41, no. 6, pp. 1918–1935, Jun. 2023.
- [9] Y. Zhang, X. Wu, and C. You, “Fast near-field beam training for extremely large-scale array,” *IEEE Wireless Commun. Lett.*, vol. 11, no. 12, pp. 2625–2629, Dec. 2022.
- [10] X. Wu, C. You, J. Li, and Y. Zhang, “Near-field beam training: Joint angle and range estimation with dft codebook,” *IEEE Trans. Wireless Commun.*, vol. 23, no. 9, pp. 11890–11903, Sep. 2024.
- [11] Q. Ziao and Y. Haifan, “A review of codebooks for csi feedback in 5g new radio and beyond,” *China Communications*, vol. 22, no. 2, pp. 112–127, 2025.
- [12] D. L. Donoho, “Compressed sensing,” *IEEE Transactions on Information Theory*, vol. 52, no. 4, pp. 1289–1306, 2006.
- [13] E. J. Candès and T. Tao, “Decoding by linear programming,” *IEEE Transactions on Information Theory*, vol. 51, no. 12, pp. 4203–4215, 2005.
- [14] J. Lee, G.-T. Gil, and Y. H. Lee, “Channel estimation via orthogonal matching pursuit for hybrid mimo systems in millimeter wave communications,” *IEEE Transactions on Communications*, vol. 64, no. 6, pp. 2370–2386, Jun. 2016.
- [15] R. Méndez-Rial, C. Rusu, N. González-Prelicic, A. Alkhateeb, and J. Heath Robert W., “Hybrid MIMO architectures for millimeter wave communications: Phase shifters or switches?” *IEEE Access*, vol. 4, pp. 247–267, 2016.
- [16] M. Rudelson and R. Vershynin, “On sparse reconstruction from fourier and gaussian measurements,” *Communications on Pure and Applied Mathematics*, vol. 61, no. 8, pp. 1025–1045, 2008.
- [17] Z. Wang, R. Kiran, S. Tsai, and R. Zhang, “Low-complexity near-field beam training with dft codebook based on beam pattern analysis,” *accepted by IEEE Globecom 2025*, Mar. 2025. arXiv: 2503.21954 [eess.SP].
- [18] Z. Wang et al., “Sparsity-aware near-field beam training via multi-beam combination,” *accepted by IEEE Globecom 2025*, 2025. arXiv: 2505.08267 [eess.SP].
- [19] Z. Wang, S. Tsai, R. Kiran, and R. Zhang, *Precise near-field beam training with dft codebook based on amplitude-only measurement*, 2025. arXiv: 2506.20783 [eess.SP].
- [20] A. Chambolle, “An algorithm for total variation minimization and applications,” *Journal of Mathematical Imaging and Vision*, vol. 20, no. 1–2, pp. 89–97, 2004.